



Microstructure, Mechanical and Corrosion Properties of Resistance Spot Welded 316 Stainless Steel Joints: The Effect of Welding Current

Sayed Rouhollah Mousavi^{1*}, Mojtaba Esmailzadeh², Ali Sabea Hammood³

¹ **Department of Materials Science and Engineering, Faculty of Engineering, Shahid Chamran University of Ahvaz, Ahvaz, Iran**

² **Department of Mechanical Engineering, Persian Gulf University, Bushehr, 75169, Iran**

³ **Department of Materials Engineering, Faculty of Engineering, University of Kufa, Najaf, Iraq**

Received: 2021-12-06, Revised: 2022-06-26, Accepted for publication: 2022-07-04

* Corresponding author: name ([E-mail](mailto:mousavirooholla@gmail.com)): mousavirooholla@gmail.com

© Published by Shahid Chamran University of Ahvaz.

Abstract

In this study, resistance spot welding (RSW) of 316 stainless steel has been studied, focusing on the welding current (10, 15, and 18 kA) and its impact on the microstructure, mechanical, and corrosion properties. The laboratory verification of welding joints has been achieved by studying the mechanical behavior of welded joints using the tensile–shear tests. Microstructure examination has been done using optical microscopy (OM), surface morphology characterization using scanning electron microscopy (SEM). The corrosion behavior of weld joints has been studied using a potentiodynamic polarization (PD) technique in a 3.5 wt. % NaCl solution. Evaluation of the welded joints indicated that corrosion resistance of RSW joint at 15 kA welding current is higher than that of other joints, whereas the corrosion rate of RSW

joint at 10 kA welding current is less than that of RSW joint at 18 kA welding current. In the presence of ferrite phase, mechanical and corrosion properties improved.

Keywords: 316 Stainless steel, Resistance spot welding, Corrosion behavior, Welding current

1. Introduction

Resistance Spot Welding (RSW) is a complex process with different factors such as thermoelectricity, metallurgy, etc. This technique is widely used in equipment body manufacturing, such as in the automotive and food industry [1], [2]. It is inexpensive, clean, and fast can be automated easily. RSW is applied to the lap joint between two or more plates[3]. Overlapping plates are placed between two copper electrodes, and heat is generated by passing a large current from the electrodes toward the plates. Resistance spot welded region is created due to electrical resistance at the plates interface and mechanical pressing of plates by electrodes in a short period, [4], [5]. The quality of RSW depends on various welding parameters such as the shape of electrodes, sheets geometry, welding time, and welding force and current during the welding process [6], [7]. RSW was used for different steels such as DP600 [8], MS1200 [9], transformation induced plasticity (TRIP) steel [4], twinning induced plasticity (TWIP) steel [10], 316L [11]–[13], etc.

Among different austenitic stainless steels, 316 stainless steel (316 SS) is one of the most widely used grades. This alloy has been utilized in different industries such as food, oil, gas, etc. It is one of the low alloyed austenitic stainless steels with good mechanical properties, decorative appearance, and high corrosion resistance [13], [14]. In addition, it shows significant weldability by optimum parameters in various welding techniques [15]. However, the main weakness of 316 SS is the reduction of corrosion resistance in welded joints such as heat-affected zone (HAZ) [16]. The inter-granular Cr-rich carbide precipitation is important for reducing corrosion resistance of austenitic grades [17], [18]. The formation of intermetallic compounds is another major weakness of welded 316 SS [19], [20]. Various factors affect the corrosion resistance of welded austenitic stainless steels, the type of welding technique is one of the most important [14].

Cui et al. [20] have reported that austenite is the preferential phase for corrosion in welded 316 SS by shield metal arc welding (SMAW). Dadfar et al. [21] concluded that tungsten inert gas (TIG) welding would reduce the corrosion resistance of 316L. Sanford et al. [22] examined the hot corrosion behavior of welded 316 SS by Active Tungsten Inert Gas (ATIG). They resulted that ATIG can increase the hot corrosion resistance of 316 SS in weld regions. Therefore,

welding metallurgy of arc welding on austenitic stainless steel joints has been well studied [23]–[27]. However, arc welding techniques introduce special features such as inclusions and other defects, reducing the corrosion resistance of weld regions of austenitic stainless steel such as 316 SS.

In addition, the literature shows that changing the welding process in many cases can significantly affect the corrosion behavior of stainless steel. Pouranvari et al. [13] maintained that there is limited research on the RSW of stainless steel. So they examined the weldability of these steels by this process. Most publications have investigated the effect of RSW parameters on the mechanical properties of austenitic stainless steels [11], [28]–[31]. Kinnersi et al. [11] optimized the RSW parameters of 316L to obtain better mechanical properties. Liu et al. [29] addressed that fatigue properties of RSWed austenitic stainless steel such as 301LN are highly dependent on RSW parameters. Vignesh et al. [32] studied the dissimilar welded 316L/DSS 2205 by RSW. The narrow Heat-affected Zone (HAZ) was observed on the 316L side. Therefore, mechanical properties have not been significantly reduced. Moshayedi et al. [30] reported that the welding current was an important parameter in the RSW of austenitic stainless steels. Recently, Hafez [25] studied the pitting corrosion behavior of RSWed 304L in various environments. The effect of the welding atmosphere on the pitting corrosion behavior was examined. The report shows that the heat input is more effective than the welding atmosphere on pitting corrosion properties of RSWed 304L.

However, there are limited studies on the corrosion behavior of RSWed of 316 SS austenitic stainless steel. To the best of the author's knowledge, quite a few studies have been carried out concerning the effect of the RSW process on the mechanical and corrosion behavior of 316 SS. In this regard, investigation of the welding process and the properties of the welded joints is indispensable and critical in each manufacturing procedure. The effects of heat input due to welding current have been evaluated on the microstructure, mechanical properties, and corrosion behavior of 316 SS to determine optimum conditions. For this purpose, different samples were welded with different welding currents and have been thoroughly examined.

2. Materials and Methods

In this study 316 austenitic stainless steel sheet with thickness of 1.5 mm was used as the base metal for RSW process. **Table 1** shows the chemical composition of this steel obtained by W6 CCD optical emission spectrometer.

Table 1 Chemical Composition of 316 SS. (wt. %)

Fe	C	Cr	Ni	Mn	Mo	P	S	Si
Balance	0.05	17.1	12.4	1.4	2.2	0.02	0.02	0.12

Stainless steel sheets were cut specimens with dimensions of 70×50 mm. The annealed material possesses the ultimate tensile strength and elongation of about 500 MPa and 38, respectively. The spot welding was performed using a typical pneumatic RSW machine (MST 200, fabricated by Pars Paya WI Co.) with high power capacity and the water cooling (25 l/min) copper electrodes. The surface of sheets was prepared by polishing and cleaning before the welding procedure in all samples; welding time and force were kept constant at 10 s and 500 Kg, respectively. The welding current was set in 10, 14, and 18 kA.

Three trials for each specimen were conducted at different welding currents. In all welding trials, the electrode force was constant. The welding conditions of specimens are listed in **Table 2**.

Table 2 Specimens and RSW Parameters

Samples	Current (kA)	Time (s)
A	10	3
B	15	3
C	18	3

Tensile–shear tests were conducted to study the mechanical behavior of the RSWed specimens. The specimens were prepared according to ASTM D638-03 standard. So, RSWed specimens had 38 mm overlap. Moreover, tensile tests were carried out at a crosshead speed of 1 mm/min by a universal testing machine UTM- Hounsfield (HLOKS). According to ISO 6507-1 micro-hardness test (by Vexus MHV-1000Z) was made across the base metal (BS), heat affected zone (HAZ), and nugget zone (NZ) at a load of 300 g for 3 s.

Feritscope FMP30 was used to measure the ferrite content of samples. The metallography examinations were carried out using an optical microscope (OM, MEIJI IM 7200) and a scanning electron microscope (SEM, LEO 1455 VP). For this work, all specimens were mounted in a certain size before they were ground and polished by different emery papers and felt, respectively. A mix solution of 45 mg ferric chloride, 9 mg copper ammonium chloride, 150 ml hydrochloric acid, 75 ml distilled water was utilized as an etchant. The average grain size was determined by ImageJ analyzing software.

The potentiodynamic polarization technique was conducted at room temperature in a 3.5 wt. % NaCl solution to examine corrosion behavior. The potential was scanned from -350mV concerning Open Circuit Potential up to 1 V. The potential scan rate was selected 1 mV/s. All potential was referred to the saturated calomel electrode (SCE) as a reference electrode. The counter electrode was a platinum electrode.

3. Results and Discussion

3.1. Microstructure Characteristics

Fig. 1 shows a schematic of indentation depth, nugget diameter, and weld penetration for RSW processing. The measured dimensions are listed in **Table 3**. The permeable indentation depth is between 20-80% of the plate thickness in RSW processing. Accordingly, the indentation depth of all-welded specimens is acceptable. It can be seen that the indentation depth has a direct relation with increasing the welding current. At a higher welding current, the weld penetration has increased, and the welding machine's jaws have become closer to each other.

For this reason, the indentation depth has increased. The same results can be seen in published research by Khuenkaew et al. [32]. It can be concluded that the welding current has many effects on the shape of the weld area.

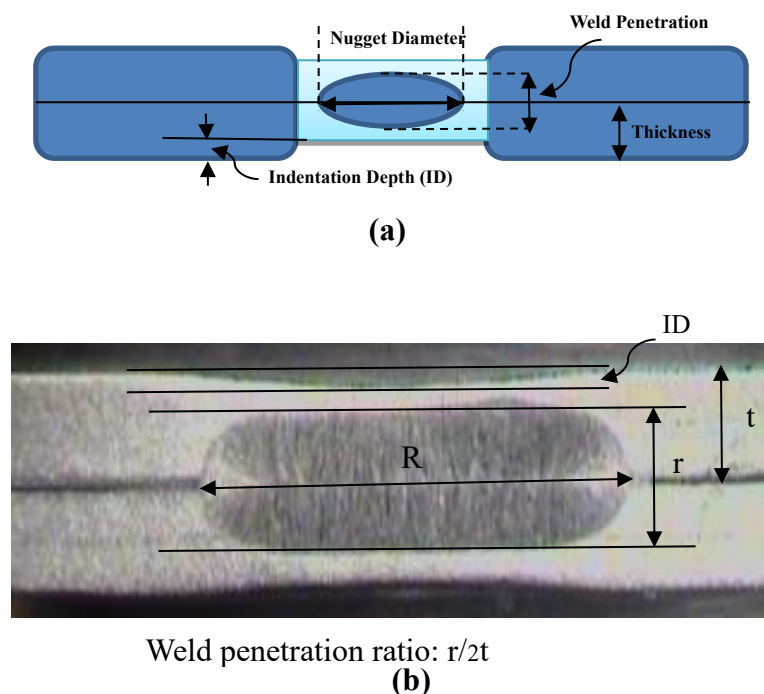


Fig. 1 Position of different zones in RSW a) schematic b) real

Table 3 Dimensional characteristics of the RSWed Samples

	Sample A	Sample B	Sample C
Indentation depth (mm)	0.35	0.37	0.42
Diameter of Weld Nugget (mm)	5.9	6	6.3
Total Thickness after Welding (mm)	2.9	2.85	2.7
Weld penetration ratio	0.67	0.73	0.77

SEM and OM images of the base metal (BM) have been shown in **Fig. 2a** and **Fig. 2b**, respectively. It can be observed that the BM has annealed and uniform grains of the austenite phase are composed. Except for the Ferrite phase, no precipitation was observed. The ferritoscropy results of BM indicated an average of 0.42% ferrite in the microstructure of 316 SS. Therefore, the structure of BM was completely.

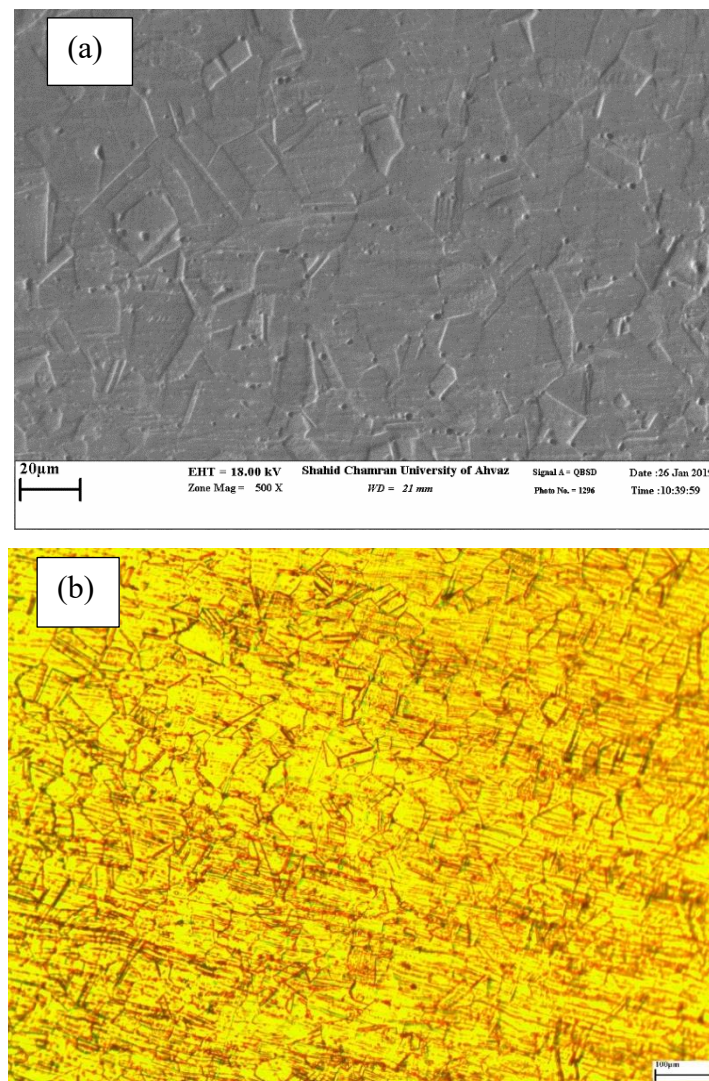
**Fig. 2** Images of Base Metal of 316 Stainless Steel: a) SEM and b) OM

Fig. 3 shows the macro and microstructure of RSWed 316 SS at 10, 15, and 18 kA welding current. It can be seen that the nugget zones have an elliptical shape in various sizes. As the welding current increases from 10 to 18 kA, the weld nugget's diameter also increases from 5.9 to 6.3 mm, respectively. The intensification of heat input is the main reason for this phenomenon.

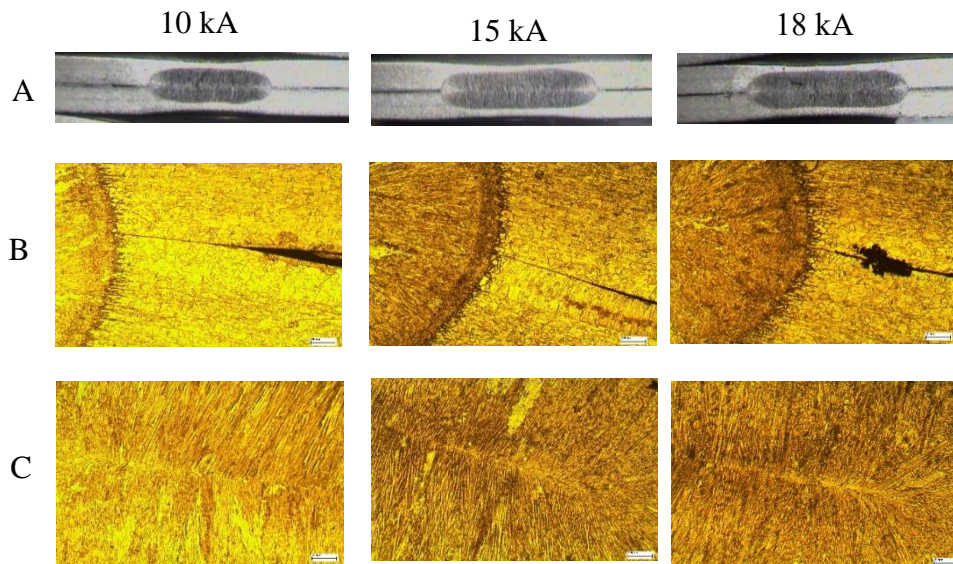


Fig. 3 Macro and microstructures of RSWed 316 samples A) Macrostructure B) HAZ C) FZ

Fig. 4 shows a high magnification of the fusion zone (FZ) of sample A. It can be seen that a large cavity has been formed in the center of FZ. This phenomenon can have two main reasons: insufficient welding force and solidification shrinkage [33]. Since most welding force is concentrated in the welding center, the cavity, due to insufficient welding force, does not form exactly in the center of FZ. Conversely, a shrinkage cavity is formed in the center of FZ.

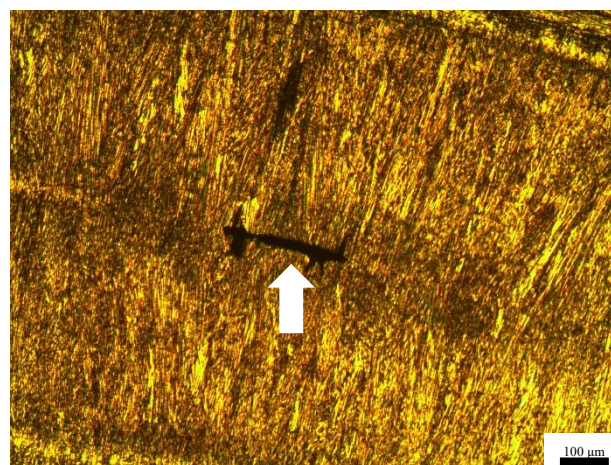


Fig. 4 OM Image of FZ Center of Sample A (10 kA)

A more detailed study of the subject based on the WRC-1992 diagram and the Eq. (1) and (2) [34]:

$$Cr_{eq} = Cr + Mo + 0.7 Nb \quad (1)$$

$$Ni_{eq} = Ni + 35 C + 20 N + 0.25 Cu \quad (2)$$

In this work, Cr_{eq} and Ni_{eq} values are 19.3 and 14.15, respectively. It is observed that for $Cr / Ni = 1.36$, the type of austenitic-ferrite solidification (AF) is changed to the austenitic type (A) with increasing solidification rate. This can lead to increased sensitivity to solidification cracks. Therefore, the evidence and studies confirm the formation of solidification cracks.

Microstructural images obtained from different regions indicate the emergence of new microstructures, which has led to the formation of HAZ and FZ (**Fig. 3**). The FZ area has two different structures indicated by FZ1 & FZ2 in **Fig. 5**. FZ1 has epitaxial growth in the FZ/HAZ interface, and FZ2 has needle austenite to the center of FZ.

Fig 3 (B) illustrates the Heat-affected Zone (HAZ) of welded specimens. As it can be seen, the width of this region is very small. However, the grain size of this area has increased compared to the BM.

Fig. 5 Fig. shows the relative position of HAZ in different welding currents. A narrow HAZ region is located between BM and FZ in 316 SS. The low thermal conductivity of 316 SS 35 is the main reason for this case. In addition, due to the element separation and accumulation of impurities, the liquid layers are formed along the grain boundaries. This phenomenon led to fluid cracking in this region. **Fig. 6** illustrates the liquid cracking for welded 316 stainless steel with 18 kA. It is reported that the absence of the ferrite phase led to fluid cracking in the grain boundaries of HAZ [13]. It appears that elements such as aluminum have low solubility in iron or some elements with high activity tend to accumulate in the grain boundaries at high temperatures. Therefore, the regions with low melting points are formed in HAZ.

The results showed that sample B has the highest ferrite value in the welding area. The main reason for this phenomenon is the difference in the method and solidification rate of samples during welding. It seems that sample B performed better in forming the ferrite phase. Proper ferrite formation can greatly improve the mechanical properties and corrosion resistance of 316 SS. The same results have been reported for other austenitic stainless steels [34].

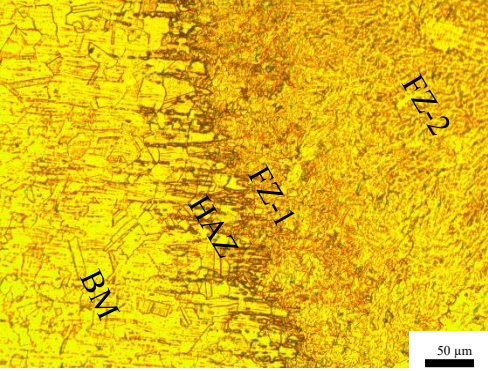
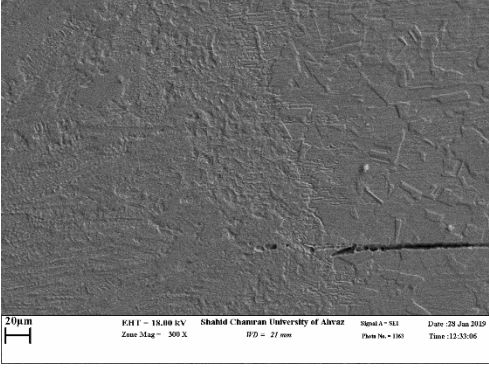
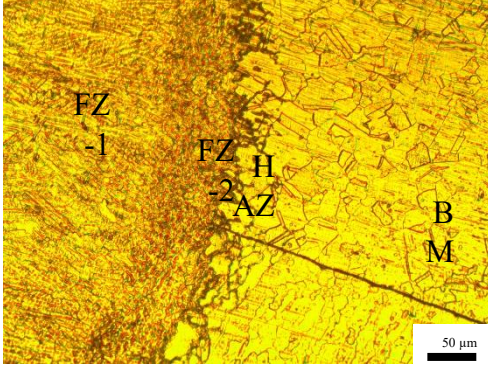
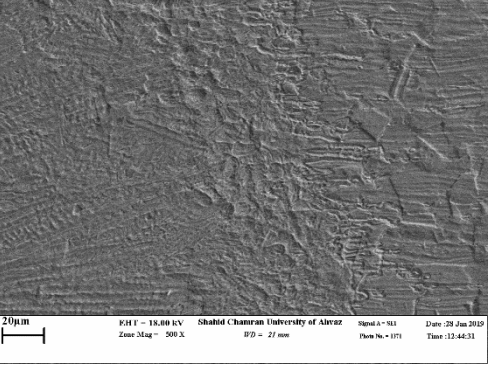
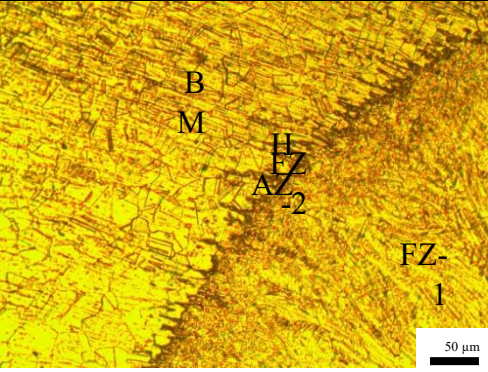
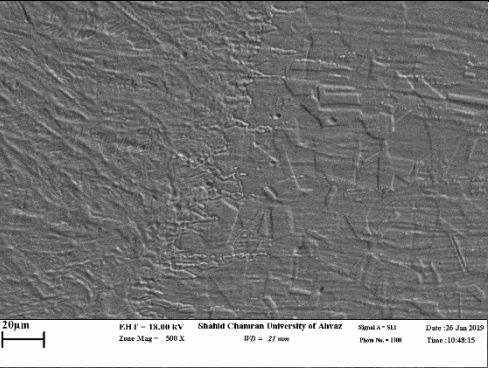
Sample	OM Image	SEM Image
A	 <p>OM Image of Sample A showing BM, HAZ, FZ-1, and FZ-2 regions. Scale bar: 50 μm.</p>	 <p>SEM Image of Sample A showing surface morphology. Scale bar: 20 μm.</p>
B	 <p>OM Image of Sample B showing FZ-1, HAZ, AZ, and BM regions. Scale bar: 50 μm.</p>	 <p>SEM Image of Sample B showing surface morphology. Scale bar: 20 μm.</p>
C	 <p>OM Image of Sample C showing BM, HAZ, AZ-2, and FZ-1 regions. Scale bar: 50 μm.</p>	 <p>SEM Image of Sample C showing surface morphology. Scale bar: 20 μm.</p>

Fig. 5 Heat-affected Zones of Three Samples A) 10 kA, B) 15 kA, and C) 18 kA

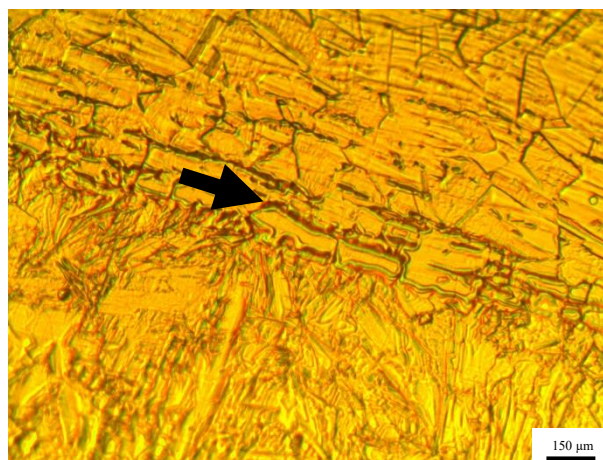


Fig. 6 OM Image of Liquid Crack of HAZ in 18 kA Specimen

3.2. Tensile – Shear Tests

It is believed that the spot-welding parameters like current have a great effect on the strength of the weld joint. It is reported that an increase in the welding current enhances the tensile load [10]. But, Razmpoosh et al. [9] showed a remarkable drop in the tensile load, and the welded samples will fail rapidly in the tensile–shear testing. It can be seen that the highest peak load of 3 kN is achieved in 15 and 10 kA welded specimens. Hence, it can be specified that the highest strength capacity of the spot weld would be obtained at optimum experimental current. So, the load-displacement curve of different conditions, as a criterion for defining optimum welding condition, have been illustrated in **Fig. 7**. The failure stress can be measured from the load by the following Eq. (3):

$$\sigma_f = 1.27 \frac{P_{max}}{rR} \quad (3)$$

Where, σ_f , P_{max} , r , and R are failure stress (MPa), maximum load (N), weld penetration (mm), and nugget diameter (mm), respectively. Figure 8 illustrates the changes in failure stress with current intensity. The failure stress decreased by increasing current from 10 to 18 kA. The same results have been reported by Valaee et al. [34] in modeling and simulation of RSW of steels. However, sample C resulted in a decrease of about 18.5% in failure stress compared to sample A, which is a large decrease compared to sample B. It seems that despite a decline of about 2.8% in failure stress of sample B, the larger dimension of the Fusion Zone (FZ) can provide maximum load and displacement. So, according to the results, sample B conditions were optimal to produce high strength spot joint in 316 SS. Ruptured samples are shown in Figure 9. Examination of ruptured samples showed that the interface of HAZ/FZ was the failure region under tensile load for samples A and B. This zone is highly prone to rupture due to the large microstructural differences between FZ and HAZ and the higher strength of FZ than the base metal. Sample C has been fractured from the FZ area. In other words, the base metal has not failed.

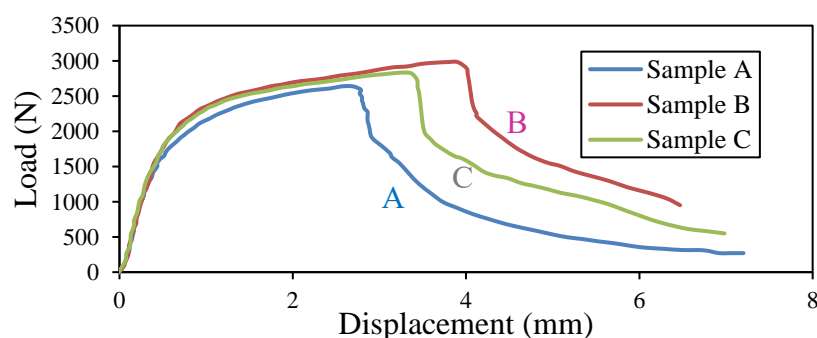


Fig. 7 Load- displacement of RSWed Specimens

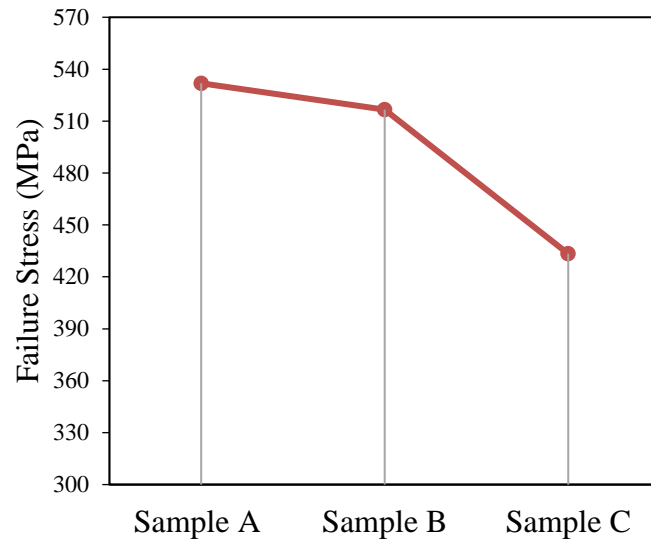


Fig. 8 Calculated Failure Stress for Different Samples

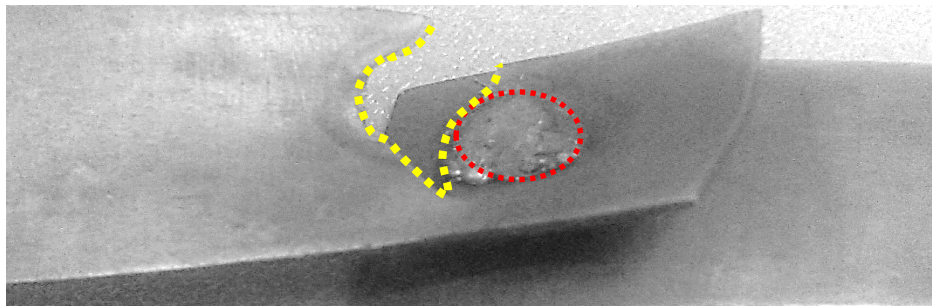


Fig. 9 The Failure Location of the Specimens during the Tensile Test

3.3. Effect of Weld Current on Corrosion Behavior

3.3.1 Corrosion Resistance Evaluation by Tafel Extrapolation

Fig. 10 shows the graphical representation of Tafel extrapolation to estimate corrosion potential (E_{corr}) and current density (i_{corr}) from potentiodynamic polarization curves (PDC). The PDC of different welds in weld current are obtained in aerated 3.5 % NaCl solution at 25 °C. The E_{corr} and i_{corr} were obtained from these curves by Tafel extrapolation. Tafel extrapolation also yields anodic and cathodic polarization slopes, the values of β_a and β_c are shown in **Table 4**.

Table 4 Potentiodynamic Polarization Data of Welded 316 SS at Different Weld Currents

Sample Name	E_{corr} (mV)	i_{corr} ($\mu\text{A}/\text{cm}^2$)	β_a (mV/decade)	β_c (mV/decade)	R_p ($\text{ohm}.\text{m}^2$)	CR (mpy)
A	-200	0.3	86	-60	5.1	0.155
B	-250	0.05	70	-35	46.7	0.026
C	-100	1	50	-40	2.2	0.515

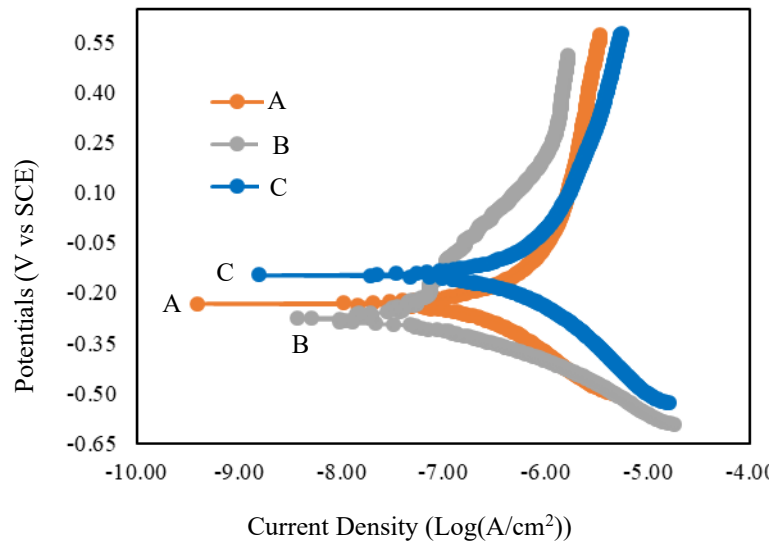


Fig. 10 Potentiodynamic Polarization Curves of Welded 316 SS at Different Weld Current.

The electrochemical reactions at the 316 SS surface in chloride ions are anodic reactions (dissolution of Fe, Cr, and Ni) and cathodic reactions (oxygen reduction). It was observed that 316 SS welded joints passive film from over the surface of welded joints is destroyed due to Cl^- . It is known that alloying elements in 316 SS play an important role in stabilizing the phases and, therefore, they can impact on the corrosion behavior of welded alloy. It was reported that smaller grains promote passive film formation, which increases with decrease in grain size. The increase in Cr content exhibits stable passive in anodic part of polarization curve exhibited passivity. The difference among polarization curves for various specimens may be due to weld samples' grain size and Cr-content. The electrochemical test showed that spot weld joint corrosion resistance at a 15 kA weld current is higher than that of other joints, as shown in **Table 4**.

In contrast, the corrosion rate for the RSW joint at 10 kA weld current is less than that of the RSW joint at 18 kA weld current. The SEM micrograph analysis indicated the pitting does not appear on the spot-weld joints surface. The higher pitting potential was observed in 316 SS due to more δ -ferrite in the weld zone, causing better corrosion resistance in 3.5 wt. % NaCl.

4. Conclusions

Through the research study, the following was concluded:

- 1-When the welding current increases in RSW for 316 SS from 10 to 18 kA, the weld nugget's diameter increases from 5.9 to 6.3 mm, respectively.
- 2-The proper ferrite formation in 316 SS after RSW can greatly improve the mechanical properties and corrosion resistance.
- 3-The conditions (15 kA, 10 min.) of RSW were optimal to produce high strength spot joint in 316 SS.
- 4- The smaller grains promote passive film formation, which increases with the decrease in grain size.
- 5- Electrochemical test showed that corrosion resistance of spot weld joint at a 15 kA weld current is higher than that of other joints, whereas the corrosion rate for RSW joint at 10 kA weld current is less than the corrosion rate for RSW joint at 18 kA weld current.
- 6- The polarization resistance increases, and corrosion rate decrease with the increase of weld current.

Disclosure Statement

No potential conflict of interest was reported by the author(s).

References

- [1] S. M. Hassoni, O. S. Barrak, M. I. Ismail, and S. K. Hussein, "Effect of Welding Parameters of Resistance Spot Welding on Mechanical Properties and Corrosion Resistance of 316L," *Mater. Res.*, vol. 25, 2022, doi: 10.1590/1980-5373-mr-2021-0117.
- [2] Y. B. Li, D. L. Li, Z. Q. Lin, S. A. David, Z. Feng, and W. Tang, "Review: magnetically assisted resistance spot welding," *Sci. Technol. Weld. Join.*, vol. 21, no. 1, pp. 59–74, Jan. 2016, doi: 10.1179/1362171815Y.0000000059.
- [3] P. R. Spena, M. De Maddis, and F. Lombardi, "Mechanical Strength and Fracture of Resistance Spot Welded Advanced High Strength Steels," *Procedia Eng.*, vol. 109, pp. 450–456, 2015, doi: 10.1016/j.proeng.2015.06.262.

- [4] M. T. N. & T. L. D. T. Van Nhat Nguyen, Van Thoai Le, *Optimization of the Resistance Spot Welding Parameters for Aluminum - Steel Weld Joint by Using the Taguchi Method*. 2022.
- [5] M. H. Bina, M. Jamali, M. Shamanian, and H. Sabet, "Investigation on the resistance spot-welded austenitic/ferritic stainless steel," *Int. J. Adv. Manuf. Technol.*, vol. 75, no. 9–12, pp. 1371–1379, Dec. 2014, doi: 10.1007/s00170-014-6220-x.
- [6] S. Ha, S. P. Murugan, K. P. Marimuthu, Y. Park, and H. Lee, "Estimation of lobe curve with material strength in resistance projection welding," *J. Mater. Process. Technol.*, vol. 263, pp. 101–111, Jan. 2019, doi: 10.1016/j.jmatprotec.2018.07.037.
- [7] M. Eshraghi, M. A. Tschopp, M. Asle Zaeem, and S. D. Felicelli, "Effect of resistance spot welding parameters on weld pool properties in a DP600 dual-phase steel: A parametric study using thermomechanically-coupled finite element analysis," *Mater. Des.*, vol. 56, pp. 387–397, Apr. 2014, doi: 10.1016/j.matdes.2013.11.026.
- [8] M. Pouranvari, S. Sobhani, and F. Goodarzi, "Resistance spot welding of MS1200 martensitic advanced high strength steel: Microstructure-properties relationship," *J. Manuf. Process.*, vol. 31, pp. 867–874, Jan. 2018, doi: 10.1016/j.jmapro.2018.01.009.
- [9] M. H. Razmpoosh, M. Shamanian, and M. Esmailzadeh, "The microstructural evolution and mechanical properties of resistance spot welded Fe–31Mn–3Al–3Si TWIP steel," *Mater. Des.*, vol. 67, pp. 571–576, Feb. 2015, doi: 10.1016/j.matdes.2014.10.090.
- [10] D. Kianersi, A. Mostafaei, and A. A. Amadeh, "Resistance spot welding joints of AISI 316L austenitic stainless steel sheets: Phase transformations, mechanical properties and microstructure characterizations," *Mater. Des.*, vol. 61, pp. 251–263, Sep. 2014, doi: 10.1016/j.matdes.2014.04.075.
- [11] A. Kajzer, W. Kajzer, K. Gołombek, M. Knol, J. Dzielicki, and W. Walke, "Corrosion Resistance, EIS and Wettability of the Implants Made of 316 LVM Steel Used in Chest Deformation Treatment," *Arch. Metall. Mater.*, vol. 61, no. 2, pp. 767–770, Jun. 2016, doi: 10.1515/amm-2016-0130.
- [12] M. Pouranvari, M. Alizadeh-Sh, and S. P. H. Marashi, "Welding metallurgy of stainless steels during resistance spot welding Part I: fusion zone," *Sci. Technol. Weld.*

- Join.*, vol. 20, no. 6, pp. 502–511, Aug. 2015, doi: 10.1179/1362171815Y.0000000015.
- [13] A. Toppo, M. G. Pujar, N. Sreevidya, and J. Philip, “Pitting and stress corrosion cracking studies on AISI type 316N stainless steel weldments,” *Def. Technol.*, vol. 14, no. 3, pp. 226–237, Jun. 2018, doi: 10.1016/j.dt.2018.03.004.
- [14] G. Rogalski, A. Świerczyńska, M. Landowski, and D. Fydrych, “Mechanical and Microstructural Characterization of TIG Welded Dissimilar Joints between 304L Austenitic Stainless Steel and Incoloy 800HT Nickel Alloy,” *Metals (Basel)*, vol. 10, no. 5, p. 559, Apr. 2020, doi: 10.3390/met10050559.
- [15] M. Landowski, A. Świerczyńska, G. Rogalski, and D. Fydrych, “Autogenous Fiber Laser Welding of 316L Austenitic and 2304 Lean Duplex Stainless Steels,” *Materials (Basel)*, vol. 13, no. 13, p. 2930, Jun. 2020, doi: 10.3390/ma13132930.
- [16] P. De Tiedra, Ó. Martín, M. López, and M. San-Juan, “Use of EPR test to study the degree of sensitization in resistance spot welding joints of AISI 304 austenitic stainless steel,” *Corros. Sci.*, vol. 53, no. 4, pp. 1563–1570, Apr. 2011, doi: 10.1016/j.corsci.2011.01.036.
- [17] Ó. Martín, P. De Tiedra, M. López, and M. San-Juan, “Combined Effect of Resistance Spot Welding and Post-Welding Sensitization on the Pitting Corrosion Behavior of AISI 304 Stainless Steel,” *CORROSION*, vol. 69, no. 3, pp. 268–275, Mar. 2013, doi: 10.5006/0749.
- [18] T. Ramkumar, M. Selvakumar, P. Narayanasamy, A. A. Begam, P. Mathavan, and A. A. Raj, “Studies on the structural property, mechanical relationships and corrosion behaviour of Inconel 718 and SS 316L dissimilar joints by TIG welding without using activated flux,” *J. Manuf. Process.*, vol. 30, pp. 290–298, Dec. 2017, doi: 10.1016/j.jmapro.2017.09.028.
- [19] A. R. Loureiro, B. F. O. Costa, A. C. Batista, and A. Rodrigues, “Effect of activating flux and shielding gas on microstructure of TIG welds in austenitic stainless steel,” *Sci. Technol. Weld. Join.*, vol. 14, no. 4, pp. 315–320, May 2009, doi: 10.1179/136217108X347610.
- [20] Y. Cui and C. D. Lundin, “Austenite-preferential corrosion attack in 316 austenitic

- stainless steel weld metals,” *Mater. Des.*, vol. 28, no. 1, pp. 324–328, Jan. 2007, doi: 10.1016/j.matdes.2005.05.022.
- [21] M. Dadfar, M. H. Fathi, F. Karimzadeh, M. R. Dadfar, and A. Saatchi, “Effect of TIG welding on corrosion behavior of 316L stainless steel,” *Mater. Lett.*, vol. 61, no. 11–12, pp. 2343–2346, May 2007, doi: 10.1016/j.matlet.2006.09.008.
- [22] B. Rebin Sanford *et al.*, “Studies on hot corrosion behaviour of A-TIG welded AISI 316 weldments,” *Mater. Today Proc.*, vol. 5, no. 5, pp. 13334–13339, 2018, doi: 10.1016/j.matpr.2018.02.325.
- [23] S. Gupta and S. Anand, “Induction of pitting corrosion on stainless steel (grades 304 and 316) used in dairy industry by biofilms of common sporeformers,” *Int. J. Dairy Technol.*, vol. 71, no. 2, pp. 519–531, May 2018, doi: 10.1111/1471-0307.12444.
- [24] E. M. Westin, “Hot cracking in duplex stainless steel weldments — a review,” *Weld. World*, vol. 66, no. 8, pp. 1483–1499, Aug. 2022, doi: 10.1007/s40194-022-01310-8.
- [25] K. M. Hafez, “The effect of welding atmosphere on the pitting corrosion of AISI 304L resistance spot welds,” *Int. J. Adv. Manuf. Technol.*, vol. 97, no. 1–4, pp. 243–251, Jul. 2018, doi: 10.1007/s00170-018-1915-z.
- [26] R. Kant, R. Mittal, C. Kumar, B. S. Rana, M. Kumar, and R. Kumar, “Fabrication and Characterization of Weldments AISI 304 and AISI 316 Used in Industrial Applications,” *Mater. Today Proc.*, vol. 5, no. 9, pp. 18475–18481, Jul. 2018, doi: 10.1016/j.matpr.2018.06.189.
- [27] D. Mishra *et al.*, “Mechanical Characterization of Monel 400 and 316 Stainless Steel Weldments,” *Procedia Eng.*, vol. 75, pp. 24–28, 2014, doi: 10.1016/j.proeng.2013.11.005.
- [28] W. Liu, R. Wang, J. Han, X. Xu, and Q. Li, “Microstructure and mechanical performance of resistance spot-welded cold-rolled high strength austenitic stainless steel,” *J. Mater. Process. Technol.*, vol. 210, no. 14, pp. 1956–1961, Nov. 2010, doi: 10.1016/j.jmatprotec.2010.07.008.
- [29] H. Moshayedi and I. Sattari-Far, “Numerical and experimental study of nugget size growth in resistance spot welding of austenitic stainless steels,” *J. Mater. Process. Technol.*, vol. 212, no. 2, pp. 347–354, Feb. 2012, doi:

- 10.1016/j.jmatprotec.2011.09.004.
- [30] H. Moshayedi and I. Sattari-Far, “Resistance spot welding and the effects of welding time and current on residual stresses,” *J. Mater. Process. Technol.*, vol. 214, no. 11, pp. 2545–2552, Nov. 2014, doi: 10.1016/j.jmatprotec.2014.05.008.
- [31] K. Vignesh, A. Elaya Perumal, and P. Velmurugan, “Optimization of resistance spot welding process parameters and microstructural examination for dissimilar welding of AISI 316L austenitic stainless steel and 2205 duplex stainless steel,” *Int. J. Adv. Manuf. Technol.*, vol. 93, no. 1–4, pp. 455–465, Oct. 2017, doi: 10.1007/s00170-017-0089-4.
- [32] Khuenkaew and Kanlayasiri, “Resistance Spot Welding of SUS316L Austenitic/SUS425 Ferritic Stainless Steels: Weldment Characteristics, Mechanical Properties, Phase Transformation and Solidification,” *Metals (Basel)*, vol. 9, no. 6, p. 710, Jun. 2019, doi: 10.3390/met9060710.
- [33] D. J. K. .C. Lippold, *Welding metallurgy and weldability of stainless steels*. 2005.
- [34] M. Valaee, M. Sheikhi, Y. M. Idu, L. Wkh, D. Idwruv, and V. Lv, “Resistance Spot Welding of Steels : Modeling and Simulation,” *Int. J. Iron Steel Soc. Iran*, vol. 14, no. 1, pp. 10–16, 2017, [Online]. Available: https://journal.issiran.com/article_26180.html